Analytic and directional wavelet packets

Amir Z. Averbuch
Sch. of Computer Science
Tel Aviv University
Tel Aviv, Israel
Email: amir1@tauex.tau.ac.il

Pekka Neittaanmäki
Dept. of Math. Information Technology
University of Jyväskylä
Jyväskylä, Finland
Email: pn@jyu.fi

Valery A. Zheludev
Sch. of Computer Science
Tel Aviv University
Tel Aviv, Israel
Email: zhel@tauex.tau.ac.il

***Abstract*—The paper presents a versatile library of analytic and quasi-analytic complex-valued wavelet packets (WPs) which originate from discrete splines of arbitrary orders. The real parts of quasi-analytic WPs are the regular spline-based orthonormal WPs designed in [1]. The imaginary parts are the so-called complementary orthonormal WPs, which, unlike the symmetric regular WPs, are antisymmetric. Tensor products of 1D quasi-analytic WPs provide a diversity of 2D WPs oriented in multiple directions. For example, the set of fourth-level WPs comprise 62 different directions. The designed computational scheme enables extremely fast and easy implementation of the WP transforms.**

I. Introduction: Analytic discrete-time periodic signals

The space of discrete-time N-periodic signals is denoted by $\Pi[N]$, and $\omega \stackrel{\text{def}}{=} e^{2\pi i/N}$. A signal $\mathbf{x} \in \Pi[N]$ is represented by its inverse DFT as follows:

$$x[k] = \frac{\hat{x}[0] + (-1)^k \hat{x}[N/2]}{N} + \frac{2}{N} \sum_{n=1}^{N/2-1} \frac{\hat{x}[n]\,\omega^{kn} + \hat{x}[n]^*\,\omega^{-kn}}{2}, \tag{1}$$

where $\cdot^*$ means complex conjugate. Note that $\hat{x}[0]$ and $\hat{x}[N/2]$ are real-valued.

Define the real-valued signal $\mathbf{y} \in \Pi[N]$ and the complex-valued signals $\mathbf{z}_+$ and $\mathbf{z}_-$:

$$y[k] \stackrel{\text{def}}{=} \frac{2}{N} \sum_{n=1}^{N/2-1} \frac{\hat{x}[n]\,\omega^{kn} - \hat{x}[n]^*\,\omega^{-kn}}{2i}, \tag{2}$$

$$z_\pm[k] \stackrel{\text{def}}{=} x[k] \pm iy[k] = \frac{\hat{x}[0] + (-1)^k \hat{x}[N/2]}{N} + \frac{2}{N} \sum_{n=1}^{N/2-1} \begin{cases} \hat{x}[n]\,\omega^{kn}, & \text{for } z_+; \\ \hat{x}[n]^*\,\omega^{-kn}, & \text{for } z_-. \end{cases} \tag{3}$$

The signal's $\mathbf{z}_+$ DFT spectrum is

$$\hat{z}_+[n] = \begin{cases} \hat{x}[n], & \text{if } n = 0, \text{ or } n = N/2\ ; \\ 2\hat{x}[n], & \text{if } 0 < n < N/2; \\ 0, & \text{otherwise} \end{cases}$$

and similarly for $\mathbf{z}_-$. The signal $\mathbf{y}$ is a discrete periodic version of the Hilbert transform (HT) of the signal $\mathbf{x} \in \Pi[N]$. The spectrum of $\mathbf{z}_+$ comprises only non-negative frequencies and vice versa for $\mathbf{z}_-$. Apparently, $\mathbf{x} = \mathfrak{Re}(\mathbf{z}_\pm)$ and $\mathfrak{Im}(\mathbf{z}_\pm) = \pm\mathbf{y}$. The signals $\mathbf{z}_\pm$ are referred to as periodic analytic signals.

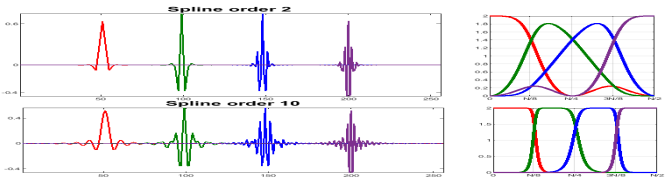

Fig. 1. Left: second-level discrete-spline WPs of orders second (top) and tenth (bottom). Right: magnitude DFT spectra of these WPs

A polar representation of the signals $\mathbf{z}$ is $z_\pm[k] = \zeta[k]\, e^{\pm\varphi[k]}$, where $\zeta[k] \stackrel{\text{def}}{=} \sqrt{x[k]^2 + y[k]^2}$ is the instantaneous amplitude of the signal $\mathbf{z}$ (envelope), and $\pm\varphi[k]\varphi[k] \stackrel{\text{def}}{=} \arctan \frac{\pm y[k]}{x[k]}$ is the instantaneous phase of $\mathbf{z}_\pm$. Since $\mathbf{x} = \mathfrak{Re}(\mathbf{z})$, we have $\mathbf{x}$ represented by $x[k] = \zeta[k]\, \cos(\varphi[k])$.

II. Spline-based wavelet packets

We designed a library of orthonormal wavelet packets (WPs) in the space $\Pi[N]$ using filters derived from continuous and discrete splines (see [1]). Although, theoretically the WPs have infinite support, they are well localized in the time domain. Their DFT spectra are flat and their shapes tend to rectangles when the orders of generating splines increases. They provide a variety of refined splits of the frequency domain into bands of different widths, depending on the decomposition level. The waveforms are symmetric. The second-level WPs derived from discrete splines of the second and tenth orders and their magnitude spectra are displayed in Fig. 1

A scheme of fast implementation of the discrete-spline-based wavelet packet transform (WPT) is presented in [1]. The transforms are executed in the spectral domain using the Fast Fourier transform (FFT) by iterative application of critically sampled two-channel filter banks to a signal. For example, the Matlab execution of the 8-level WPT originating from the 12-th-order discrete spline, of a signal comprising 245760 samples, takes 0.2324 seconds.

a) Outline of implementation of real-valued WPT: The filter bank for the one-level transform, which originates from the discrete splines of order $2r$, is defined by its modulation

matrix

$$\mathbf{M}[n] = \sqrt{2}\begin{pmatrix} \beta_{[0]}[n] & \beta_{[0]}\left[n+\frac{N}{2}\right] \\ \alpha_{[0]}[n] & \alpha_{[0]}\left[n+\frac{N}{2}\right] \end{pmatrix}, \quad (4)$$

$$U^{4r}[n] = \frac{1}{2}\left(\cos^{4r}\frac{\pi\, n}{N} + \sin^{4r}\frac{\pi\, n}{N}\right), \quad (5)$$

$$\beta_{[0]}[n] = \frac{\cos^{2r}\frac{\pi\, n}{N}}{\sqrt{2\,U^{4r}[n]}}, \quad \alpha_{[0]}[n] = \omega^n\,\frac{\sin^{2r}\frac{\pi\, n}{N}}{\sqrt{2\,U^{4r}[n]}}. \quad (6)$$

The matrix $\mathbf{M}[n]/2$ is unitary. The one-level WPT of a signal $\mathbf{x} \in \Pi[N]$ is represented in a matrix form:

$$\begin{pmatrix} \hat{w}_{[1],0}[n] \\ \hat{w}_{[1],1}[n] \end{pmatrix} = \frac{1}{2}\mathbf{M}[-n]\cdot\begin{pmatrix} \hat{x}[n] \\ \hat{x}\,[n+N/2] \end{pmatrix}.$$

The coefficients $\left\{w_{[1],l}[k]\right\}$, $l = 0, 1$, are derived by the inverse DFT of $\left\{\hat{w}_{[1],l}[n]\right\}$.

The matrix for the transition from the first to the second decomposition level is $\mathbf{M}_{[2]}[n] = \mathbf{M}[2n]$ and so on.

The signals $\psi^{2r}_{[1],0}$ and $\psi^{2r}_{[1],1}$, whose DFTs are $\sqrt{2}\beta_{[0]}[n]$ and $\sqrt{2}\alpha_{[0]}[n]$, respectively, are the WPs of the first level. Their two-sample shifts form an orthonormal basis of the signal space $\Pi[N]$. The WPs for the subsequent decomposition levels $\left\{\psi^{2r}_{[m],l}\right\}$, where $m = 1, ..., M$ is the index of the decomposition level and $l = 0, ...2^m - 1$ is the wavelet packet's number, are derived iteratively in a conventional way. All the computations are implemented in the frequency domain using the FFT.

III. Analytic wavelet packets

A. Wavelet packets

The analytic spline-based WPs and their DFT spectra are derived from the corresponding WPs $\left\{\psi^{2r}_{[m],l}\right\}$ in line with the scheme in Section I (see Eqs. (1), (2), (3)).

Denote by $\theta^{2r}_{[m],l}$ the discrete periodic HT of the wavelet packet $\psi^{2r}_{[m],l}$. Then, the corresponding analytic WPs are

$$\bar{\psi}^{2r}_{\pm[m],l} = \psi^{2r}_{[m],l} \pm i\theta^{2r}_{[m],l}. \quad (7)$$

a) Properties:

- The DFT spectra of the analytic WPs $\bar{\psi}^{2r}_{+[m],l}$ and $\bar{\psi}^{2r}_{-[m],l}$ are located within the bands $[0, N/2]$ and $[N/2, N]$, respectively.
- Real component $\psi^{2r}_{[m],l}$ is the same for both the WPs $\bar{\psi}^{2r}_{\pm[m],l}$. It is a symmetric oscillating waveform.
- The HT WP $\theta^{2r}_{[m],l}$ is an antisymmetric oscillating waveform. Its magnitude spectrum $\left|\hat{\theta}^{2r}_{[m],l}[n]\right|$ coincides with the magnitude spectrum of the respective WPs $\psi^{2r}_{[m],l}$ everywhere except for the points $n = 0, N/2$, where it is zero.

B. Complementary set of wavelet packets

All the HP WPs $\theta^{2r}_{[m],l}$ with $l = 1, ..., 2^m - 2$ have orthonormality properties similar to the properties of the WPs $\psi^{2r}_{[m],l}$. However, this is not the case for $l = 0, 2^m - 1$. Therefore, the WPs $\theta^{2r}_{[m],l}$ with $0, 2^m - 1$ are updated to achieve the orthonormality at the expense of a slight distortion of the antisymmetry. Define a set of signals from the space $\Pi[N]$

$$\varphi^{2r}_{[m],l}[k] \stackrel{\text{def}}{=} \hat{\psi}^{2r}_{[m],l}[0]/N + \hat{\psi}^{2r}_{[m],l}[N/2]/N + \theta^{2r}_{[m],l}[k]. \quad (8)$$

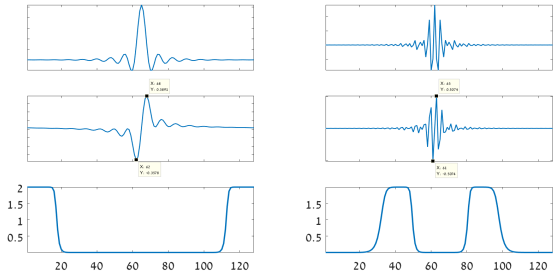

Fig. 2. Left: WPs $\psi^{10}_{[2],0}$ (top), $\varphi^{10}_{[2],0}$ (center) and magnitude DFT spectra of the latter. Right: same for the WPs $\psi^{10}_{[2],2}$ and $\varphi^{10}_{[2],2}$, respectively

Figure 2 displays the WPs $\psi^{10}_{[2],l}$, $l = 0, 2$ and $\varphi^{10}_{[2],l}$, $l = 0, 2$, from the second decomposition level and magnitude spectra of WPs $\varphi^{10}_{[2],l}$, $l = 0, 2$. The WPs are derived from tenth-order discrete splines. A deviation from the antisymmetry is seen in the WP $\varphi^{10}_{[2],0}$.

a) Properties:

- The magnitude spectra of the cWPs $\left|\hat{\varphi}^{2r}_{[m],l}[n]\right|$ coincide with the magnitude spectra of the respective WPs $\psi^{2r}_{[m],l}$.
- For any $m = 1, ..., M$, and $l = 1, ..., 2^m - 2$, the signals $\varphi^{2r}_{[m],l}$ are antisymmetric oscillating waveforms. For $l = 0$ and $l = 2^m - 1$, the shapes of the signals are near antisymmetric.
- The orthonormality properties similar to the properties of the WPs $\psi^{2r}_{[m],l}$ hold for the signals $\varphi^{2r}_{[m],l}$:

$$\left\langle \varphi^{2r}_{[m],l}[\cdot - p\,2^m], \varphi^{2r}_{[m],\lambda}[\cdot - r\,2^m] \right\rangle = \delta[\lambda, l]\,\delta[p, r]. \quad (9)$$

We refer to the signals $\left\{\varphi^{2r}_{[m],l}\right\}$, $m = 1, ..., M$, $l = 0, ..., 2^m - 1$ as *complementary wavelet packets* (cWPs). Similarly to the WPs $\left\{\psi^{2r}_{[m],l}\right\}$, differenent combinations of the cWPs can provide differenent orthonormal bases for the space $\Pi[N]$. Those can be, for example, the wavelet bases or different versions of the Best Basis [2].

b) Implementation of cWPT: is similar to the implementation of the WPT with WPs $\left\{\psi^{2r}_{[m],l}\right\}$. Denote $\tilde{\beta}_{[0]}[n] = i\,\beta_{[0]}[n]$, $n \neq 0$, $\tilde{\beta}_{[0]}[0] = \beta_{[0]}[0]$ and $\tilde{\alpha}_{[0]}[n] = i\,\alpha_{[0]}[n]$, $n \neq N/2$, $\tilde{\alpha}_{[0]}[N/2] = \alpha_{[0]}[N/2]$. The modulation matrix is

$$\tilde{\mathbf{M}}[n] = \sqrt{2}\begin{pmatrix} \tilde{\beta}_{[0]}[n] & -\tilde{\beta}_{[0]}\left[n+\frac{N}{2}\right] \\ \tilde{\alpha}_{[0]}[n] & -\tilde{\alpha}_{[0]}\left[n+\frac{N}{2}\right] \end{pmatrix}.$$

The decomposition of a signal $\mathbf{x} \in \Pi[N]$ down to M-th level produces $2MN$ transform coefficients. Such a redundancy provides many options for the signal reconstruction, such as: 1. A basis compiled from either WPs $\Psi = \left\{\psi^{2r}_{[m]}\right\}$ or $\Phi = \left\{\varphi^{2r}_{[m]}\right\}$. 2. Combination of bases compiled from

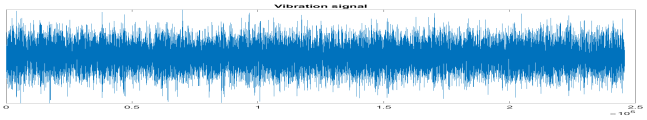

Fig. 3. Vibration signal from a slow-rotating REB

both Ψ and Φ WPs generates a tight frame of the space $\Pi[N]$ with the redundancy rate 2. The bases for Ψ and Φ can have different structure. 3. Frames with increased redundancy rate, for example a combined reconstruction from several decomposition levels. 4. In addition, the WPs and cWPs can be used as the dictionaries for the Matching Pursuit scheme.

It is worth mentioning that the generating spline's order $2r$, which determines the spectra flatness and the number of local vanishing moments, can be varied without change of the computation complexity of the transforms.

C. Quasi-analytic wavelet packets

Define the set of complex-valued WPs, which we refer to as the quasi-analytic wavelet packets:

$$\tilde{\psi}^{2r}_{\pm[m],l} = \psi^{2r}_{[m],l} \pm i\varphi^{2r}_{[m],l}, \quad m = 1, ..., M,\ l = 0, ..., 2^m - 1,$$

where $\varphi^{2r}_{[m],l}$ are the cWPs defined in Eq. (8). The WPs $\tilde{\psi}^{2r}_{\pm[m],l}$ differ from the analytic WPs $\bar{\psi}^{2r}_{\pm[m],l}$ by the addition of the two numbers $i\,\hat{\psi}^{2r}_{[m],l}[0]/N$ and $i\,\hat{\psi}^{2r}_{[m],l}[N/2]/N$. For a given decomposition level m, these numbers are zero for all l except for $l_0 = 0$ and $l_m = 2^m - 1$. It means that for all l except for l_0 and l_m the WPs $\tilde{\psi}^{2r}_{\pm[m],l}$ are analytic.

D. Application example: bearing fault detection

Due to their properties, such as (anti)symmetry, transient oscillating structure and refined frequency resolution, the spline-based WPs $\psi^{2r}_{[m],l}$ and $\varphi^{2r}_{[m],l}$ and their envelopes proved to be efficient in solving a difficult problem of the early fault detection in heavy-duty rolling element bearings (REB) via the analysis of vibration signals. The vibration signals were recorded in a real working environment. The fault produces repeating pulses, which generate high-frequency transient oscillations. The pulses repetition frequency (RF) is determined by the installment structure and the rotation speed of the REB and can be evaluated theoretically. The problem is to detect the pulses with the estimated RF (if they exist). The problem is aggravated by presence of strong noise and multiple extraneous vibrations.

The fault-related transient oscillations are confined in a certain frequency band $\mathbf{B}$. We select WPs $\psi^{2r}_{[m],l}$ and $\varphi^{2r}_{[m],l}$ from differenent decomposition levels whose spectra are located within the band $\mathbf{B}$. To catch the fault-related transient, we try to find a waveform whose shape is close to the shape of the transient and to determine its RF. It is done by application of a version of the Matching Pursuit scheme followed by the computation of the DFT spectra of the pursued signals' envelopes. In many cases, the antisymmetric waveforms $\varphi^{2r}_{[m],l}$ were advantageous over the symmetric ones $\psi^{2r}_{[m],l}$.

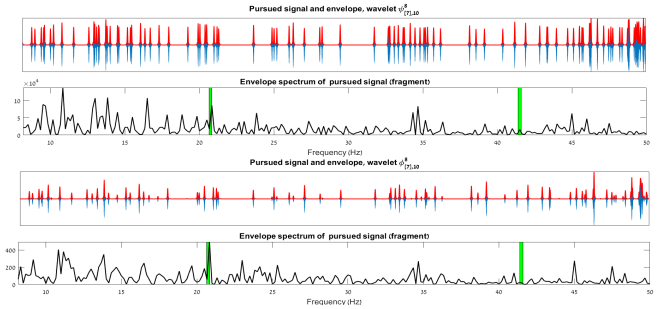

Fig. 4. Top and Second from the bottom: Results of Pursuit by WPs $\psi^8_{[7],10}$ and $\varphi^8_{[7],10}$, respectively. Second from the top and Bottom: Envelope spectra of pursued signals for WPs $\psi^8_{[7],10}$ and $\varphi^8_{[7],10}$, respectively. Green bars – theoretical RF and its overtone

Figure 4 illustrates the application the of the Matching Pursuit scheme to a vibration signal recorded from a slow-rotating REB (Fig. 3). The theoretical RF was 20.7432 Hz. The fault-related transients were captured by the WPs $\psi^8_{[7],10}$ and $\varphi^8_{[7],10}$. from the seventh decomposition level. The envelope spectra determined the RF=20.83, which is close to the theoretical RF. Comparing the bottom frame from Fig. 4 with the second from the top frame, we see that the wavelet $\varphi^8_{[7],10}$ indicates on the fault more clearly than $\psi^8_{[7],10}$.

IV. Directional 2D WPs

A. Design of directional WPs

A standard procedure for the design of two-dimensional (2D) WPs is to compute the tensor products of 1D WPs:

$$\psi^{2r}_{[m],\lambda,l}[k,n] = \psi^{2r}_{[m],\lambda}[k]\,\psi^{2r}_{[m],l}[n].$$

These 2D WPs are separable and lack a directionality. To derive a collection of 2D WPs oriented in a multiple directions, we compute the tensor products of quasi-analytic 1D WPs:

$$\begin{aligned}\tilde{\psi}^{2r}_{+[m],\lambda,l}[k,n] &= \tilde{\psi}^{2r}_{+[m],\lambda}[k]\,\tilde{\psi}^{2r}_{+[m],l}[n],\\ \tilde{\psi}^{2r}_{-[m],\lambda,l}[k,n] &= \tilde{\psi}^{2r}_{+[m],\lambda}[k]\,\tilde{\psi}^{2r}_{-[m],l}[n]\end{aligned}$$

and take real parts of these complex-valued WPs:

$$\begin{aligned}\Psi^{2r}_{\pm[m],\lambda,l}[k,n] &\stackrel{\text{def}}{=} \mathfrak{Re}(\tilde{\psi}^{2r}_{\pm[m],\lambda,l}[k,n]) \\ &= \psi^{2r}_{[m],\lambda}[k]\,\psi^{2r}_{[m],l}[n] \mp \varphi^{2r}_{[m],\lambda}[k]\,\varphi^{2r}_{[m],l}[n].\end{aligned} \tag{10}$$

Such a design is somewhat similar to the design of 2D directional wavelets in [3], [4]. Figure 5 displays directional WPs $\Psi^8_{\pm[3],\lambda,l}$ from the third decomposition level. The WPs are derived from the eighth-order discrete splines. 30 differenent directions are seen in the figure. Note that the WPs $\Psi^8_{+[3],\lambda,l}$ are oriented to *north-east*, while $\Psi^8_{+[3],\lambda,l}$ are oriented to *north-west*. The WPs from the *m*th level comprise $2 \times 2^m \times (2^m - 1)$ differenent directions.

B. Implementation of directional WPTs

If $\mathbf{X}$ is a 2D array to be processed, the two transforms with the tensor-product WPs $\psi^{2r}_{[m],\lambda,l}[k,n] = \psi^{2r}_{[m],\lambda}[k]\,\psi^{2r}_{[m],l}[n]$ and $\varphi^{2r}_{[m],\lambda,l}[k,n] = \varphi^{2r}_{[m],\lambda}[k]\,\varphi^{2r}_{[m],l}[n]$ are implemented, as

(a) (b)

Fig. 5. 2D WPs from the third decomposition level. Left: $\Psi^8_{+[3],\lambda,l}$. Left: $\Psi^8_{-[3],\lambda,l}$, $\lambda, l = 0, ..., 7$

described in [1], thus producing two coefficients arrays C_ψ and C_φ, respectively. These arrays are combined into the arrays $C_+ \stackrel{\text{def}}{=} C_\psi - C_\varphi$ and $C_- \stackrel{\text{def}}{=} C_\psi + C_\varphi$, which comprise of the transform coefficients of the array $\mathbf{X}$ with the directional WPs $\Psi^{2r}_{+[m],\lambda,l}$ and $\Psi^{2r}_{-[m],\lambda,l}$, respectively. Subsets $\bar{C}_\pm \subset C_\pm$ are selected that are associated with a certain structure $\bar{B}_\pm$ (wavelet or the Best Bases, for example) consisting of shifts of the WPs $\Psi^{2r}_{\pm[m],\lambda,l}$, respectively. In that case the WPs $\Psi^{2r}_{\pm[m],\lambda,l}$ provide a tight frame of the space $\Pi[N, N]$, with the redundancy rate 2. After some manipulations on the coefficients $\bar{C}_\pm$, such as thresholding, for example, the inverse transforms have produced the two arrays $\mathbf{X}_\pm$ associated with the WPs Ψ^{2r}_+, and Ψ^{2r}_-, respectively, which have different orientations. Therefore, neither of the arrays $\mathbf{X}_+$ and $\mathbf{X}_-$ provide full restoration of $\mathbf{X}$. A perfect reconstruction of $\mathbf{X}$ is achieved by averaging $\bar{\mathbf{X}} = (\mathbf{X}_+ + \mathbf{X}_-)/2$.

C. Application example: "Barbara" denoising

This simple example illustrates difference between the performance of directional and regular tensor-product (TP) wavelets. The directional and TP four-level wavelet transforms derived from 8-th order discrete splines are applied to the "Barbara" image affected by 30 Db Gaussian noise (PSNR =18,6 Db). The transform coefficients are soft thresholded and the images are restored in line with the above scheme. The directional transform produced better denoising and retained much more details and lines in the image than the TP one. The PSNRs are 27.18 versus 25.07 Db. Results are displayed in Fig. 6. In addition, partial reconstruction of the image by the arrays $\mathbf{X}_+$ and $\mathbf{X}_-$ is displayed in the figure.

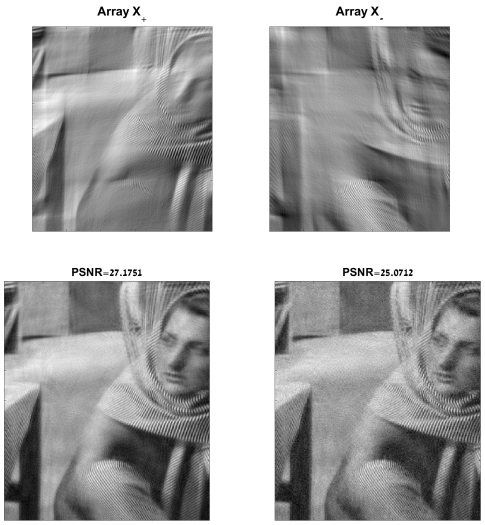

Fig. 6. Topt: Partially restored "Barbara" image by $\mathbf{X}_+$ (left) and $\mathbf{X}_-$ (right). Bottom: Fragments of the image restored from directional (left) and TP (right) wavelet transforms

V. Conclusion

We presented a scheme for the design and implementation of the spline-based analytic WPTs that, in a 2D case, generate a diversity of directional WPTs. The transforms are easy to manipulate and fast to implement. For example, MATLAB implementation of the six-level directional WPT of the 512×512 image takes 0.8 sec. Having at hand such a versatile and easily operated toolbox, we plan to apply it to variety of signal and image processing problems such as analysis of technological and biomedical signals, detection of transient events, image denoising, deblurring and inpainting, target detection and processing of hyperspectral data.

Acknowledgment

This research was partially supported by the Israel Science Foundation (ISF, 1556/17), Blavatnik Computer Science Research Fund Israel Ministry of Science and Technology 3-13601 and by Academy of Finland (grant 311514).

References

[1] A. Averbuch, P. Neittaanmäki, and V. Zheludev, *Splines and spline wavelet methods with application to signal and image processing, Volume III: Selected topics*. Springer, 2019.

[2] R. R. Coifman and V. M. Wickerhauser, "Entropy-based algorithms for best basis selection," *IEEE Trans. Inform. Theory*, vol. 38, no. 2, pp. 713–718, 1992.

[3] I. Selesnick, R. Baraniuk, and N. Kingsbury, "The dual-tree complex wavelet transform," *IEEE Signal Process. Mag.*, vol. 22, no. 6, pp. 123–151, 2005.

[4] B. Han and Z. Zhao, "Tensor product complex tight framelets with increasing directionality," *SIAM J. Imaging Sci.*, vol. 7, 2014.